Organic matter deposition and paleoenvironmental implications across the Cenomanian-Turonian boundary of the Subalpine Basin (SE France): Local and global controls

Carolina Fonseca, João Graciano Mendonça Filho, Carine Lézin, António Donizeti De Oliveira, Luís V. Duarte

Organic matter deposition and paleoenvironmental implications across the Cenomanian-Turonian boundary of the Subalpine Basin (SE France): local and global controls

Carolina Fonseca[a*], João Graciano Mendonça Filho[b], Carine Lézin[a], António Donizeti de Oliveira[b], Luís V. Duarte[c]

[a] Université Toulouse III – Paul Sabatier, OMP, GET (Géosciences Environnement Toulouse), CNRS, IRD, 14 avenue Édouard Belin, F-31400 Toulouse, France.
[b] Laboratório de Palinofácies e Fácies Orgânica (LAFO), Departamento de Geologia, Instituto de Geociências, Universidade Federal do Rio de Janeiro, Av. Athos da Silveira, 274, prédio do CCMN, sala J1020, Campus Ilha do Fundão, Cidade Universitária, CEP 21.949-900, Rio de Janeiro, RJ, Brazil.
[c] MARE - Marine and Environmental Sciences Centre, Faculty of Sciences and Technology, Department of Earth Sciences, University of Coimbra, Rua Sílvio Lima, 3030-790 Coimbra, Portugal.
*carolina.fonseca@get.omp.eu (corresponding author)

Abstract

The Cenomanian-Turonian boundary is marked by global sea-level highstands and one of the warmest periods of the Mesozoic, with high pCO_2 levels linked to a massive magmatic episode. This is associated with the establishment of a worldwide marine anoxia, the deposition of organic-rich facies and disturbances of the global carbon cycle, the so-called Oceanic Anoxic Event 2 (OAE2). The Pont d'Issole section's (Subalpine Basin, SE France) sedimentary succession represents the reference record of OAE2 in the Tethyan domain, although its organic fraction is extremely poorly studied. Therefore, the main objectives of this study are the characterization of the Pont d'Issole section's organic matter (OM) for paleoenvironmental interpretation and the assessment of the OM thermal maturity using organic petrology and organic geochemistry techniques.

The organic record characterizes a shallowing-up marine system with varying redox and restriction conditions, associated with periods of stratified oxygen regimen. It displays the presence of two OM enrichment episodes with different paleoenvironmental and geodynamic contexts. The first OM enrichment episode (Unit Th1) is thought to be associated with the global mechanisms that trigger OAE2 and is characterized by a palynofacies association co-dominated by amorphous OM and marine microplankton, reflecting a context of high sea-level. This is followed by the Plenus Cold Event (Unit Th2), characterized by a decrease in amorphous OM and increase in marine

microplankton, representing a reoxygenation associated with an increase in water level, and an apparent decrease in temperature (disappearance of *Classopollis* sp.). The second OM enrichment episode (Unit Th3 and base of Unit Th4) is characterized by an association dominated by amorphous OM, the occurrence of freshwater microplankton, and the development of a restricted environment with low sea level. These depositional conditions are thought to be connected to the beginning phases of basin closure, promoted by the regional tectonic framework (compressive trend between Africa and Europe).

The molecular fraction showed the presence of unsaturated compounds, monoaromatic steranes, monoaromatic anthrasteroids and the biological ββ hopanes, indicating a low thermal evolution for the OM. This is corroborated by biomarkers ratios and organic petrographic data, namely vitrinite reflectance (0.29% Rr).

The presence of Paleozoic reworked OM in the samples was also identified presenting a more complex thermal history than the Cretaceous OM. This OM is possibly related to the subaerial erosion of Hercynian Massifs.

Keywords: Organic facies; Palynofacies; Reworked Organic Matter; Biomarkers; Oceanic Anoxic Event 2; Pont d'Issole

1. Introduction

The Cenomanian-Turonian boundary (CTB) is characterized by extensive organic carbon burial related to worldwide bottom-water anoxia. This immense burial of ^{13}C-depleted organic matter (OM) is reflected by a positive isotopic excursion ($\delta^{13}C$ ~ 2.5‰; e.g. Scholle and Arthur, 1980; Schlanger et al., 1987; Arthur et al., 1988; Hasegawa, 1997; Tsikos et al., 2004; Jenkyns, 2010) in the signature of both marine carbonates and OM, allowing the definition of the so-called Oceanic Anoxic Event 2 (OAE2) (e.g. Schlanger and Jenkyns, 1976; Jenkyns, 2010).

During the CTB, paleogeography and high atmospheric CO_2 concentrations possibly enhanced a warm climate that restricted oxygen in the oceans and atmosphere (e.g. Pucéat et al., 2003; Takashima et al., 2006; Forster et al., 2007; Sinninghe Damsté et al., 2010; Friedrich et al., 2012; O'Brien et al., 2017). These high atmospheric and oceanic CO_2 concentrations are inferred to be linked to the contemporaneous emplacement of large igneous provinces, namely in the Caribbean and in the High Arctic (Jones and Jenkyns, 2001; Snow et al., 2005; Kuroda et al., 2007; Turgeon and Creaser, 2008; Du Vivier et al., 2014). The associated volcanic activity would therefore enhance the availability of micronutrients that contributed to an increase in primary productivity, facilitated carbon remineralization and promoted nutrient recycling (Sinton and Duncan, 1997; Leckie et al., 2002). This increase in nutrients could also be related to an enhancement of the hydrological cycle and increased terrestrial weathering (Mort et al., 2007; Frijia and Parente, 2008; Monteiro et al., 2012; Pogge von Strandman et al., 2013). It is important to emphasize that regional factors, such as paleogeomorphology and oceanic circulation dynamics, could be a determinant for the variations in the expression of this global event (Trabucho Alexandre et al., 2010; van Helmond et al., 2014; Zheng et al., 2016).

Thus, different origins are mentioned to explain the setting up of OAE2. Many geochemical studies focus on extracting the global signature of such event from the local sedimentary record (e.g. Hussler et al., 1981; Hussler and Albrecht, 1983; Sinninghe Damsté et al., 2008, 2014; Jarvis et al., 2011; Sachse et al., 2011; Ghassal et al., 2016). Although this is a necessary exercise, a detailed understanding of the sedimentary fraction is equally important, as local contexts can play a key role in the shaping of these signatures. This is even more evident when dealing with the organic fraction, as several issues are described in the literature for using exclusively organic geochemistry techniques (e.g. molecular biomarkers, Rock-Eval pyrolysis) for the characterization of the organic fraction, e.g. hydrocarbon contaminants (drilling fluids), immaturity or

overmaturity of the OM, and presence of solid bitumen (Bordenave et al., 1993; Peters and Cassa, 1994; Gonçalves et al., 2013, 2014, 2015; French et al., 2015; Sousa et al., 2019). Therefore, it is necessary to study this sedimentary fraction in order to differentiate between the global and local factors that are at the origin of its formation and deposition. Black shale deposits are the best sedimentary markers of anoxic events (e.g. Schlanger and Jenkyns, 1976; Lüning et al., 2004). This organic-rich sedimentary material, which can have a variable composition, records specific conditions of productivity, preservation and burial controlled by autocyclic (e.g. temperature, nutrients) and allocyclic factors (e.g. climate, tectonics; e.g. Schlanger and Jenkyns, 1976; Kerr, 1998; Lüning et al., 2004; Takashima et al., 2006; Trabucho Alexandre et al., 2010; Monteiro et al., 2012).

The sedimentary expression of OAE2 is well recorded in the Subalpine Basin (SE France) in the reference section of Pont d'Issole (e.g. Grosheny et al., 2006, 2017; Jarvis et al., 2011) where organic-rich sediments (including black shales), deposited in varying redox conditions, have been identified (Crumière et al., 1990; Jarvis et al., 2011; Danzelle et al., 2018). This organic-rich record is disturbed by a sequence of sediments with low organic content that is correlated to a cooling episode within OAE2, the so-called Plenus Cold Event, identified by Jarvis et al. (2011). The Pont d'Issole sedimentary succession represents the reference record of OAE2 in the Tethyan domain. This section has been intensively studied from a geochemical point of view (e.g. Morel, 1998; Grosheny et al., 2006; Takashima et al., 2009; Jarvis et al., 2011; Du Vivier et al., 2014, 2015; Danzelle et al., 2018; Raven et al., 2018; 2019), however, a detailed petrographic study of the OM composition has not been carried out. The location of this section in the distal part of a turbiditic system (Grosheny et al., 2017) is vital for the better understanding of the local sedimentary and paleoenvironmental contexts and for the definition of the local and global factors that control the establishment of anoxia.

With these premises, the aims of this study are: (i) to characterize the OM of the CTB sedimentary succession of the Pont d'Issole section, using organic geochemistry and palynofacies; (ii) to assess the thermal maturity of the OM splitting that primary from the Paleozoic reworked OM; (iii) to define depositional paleoenvironments based on the organic facies; and, (iv) to discuss the implications in terms of sedimentary and paleogeographic context and paleoenvironmental conditions.

2. Geological Setting

During the latest Cenomanian to earliest Turonian, the Subalpine Basin (or Vocontian Basin) developed as an epicontinental gulf in the European Alpine Ocean of the northern Tethyan realm, positioned at a paleolatitude of 25º–30ºN (Vocontian Trough), and bordered by the crystalline rocks of emerged Hercynian massifs (Grosheny et al., 2006, 2017; Schreiber et al., 2011; Fig. 1).

From the Aptian to the Albian the basin underwent a compression concomitant with the opening of the Bay of Biscay, with the deformation of its paleogeography by the sinistral play of strike-slip faults (Nîmes and Durance faults) and early Alpine folding phases (Grosheny et al., 2017). This led to the appearance of E-W domains (Durancian Isthmus) and deep subsiding troughs (Vocontian Trough and Lower Provence Gulf) in this transitional structural context between the collisional domain of the Pyrenees and the subduction zone that was developing in the eastern part of the basin (Alpine subduction; Schreiber et al., 2011).

The evolution and geometry of the Late Cretaceous Subalpine Basin, and, more specifically, of the Vocontian Basin, are linked to Pyrenean-Provence tectonics. This tectonic control is corroborated by numerous truncations of the series, internal unconformities, and a dominant detrital sedimentation with turbidites (Schreiber et al., 2011; Grosheny et al., 2017). The tectonic disturbances at the CTB are therefore thought to be the expression of a pulse in the compressive movement between Africa and Europe and explain the gradual eastward marine regression toward the Alpine sea recorded during the Late Cretaceous (Grosheny et al., 2017). At the same time, the initial phases of closure of the basin are recorded, culminating in the complete emersion of the basin at the end of the Late Cretaceous (Schreiber et al., 2011).

In the Subalpine Basin, the CTB sedimentation is characterized by ~20–25m of a distinct dark organic-rich facies that extend to the deepest part of the basin (Crumière, 1990; Takashima et al., 2009; Jarvis et al., 2011; Danzelle et al., 2018). The Pont d'Issole section (coordinates: 44°4'11.64''N; 6°28'58.08''E) was selected as a reference section for the CTB of the Subalpine Basin (Vocontian Trough; Figs. 1– 2). The Upper Cenomanian–Lower Turonian interval of this section is characterized by bioturbated limestones followed by an alternation of calcareous dark shales with interbedded thin gray marls (units Th1 and Th3, Jarvis et al., 2011) and highly bioturbated limestone beds with interbedded gray marlstones (units Th2 and Th4, Jarvis et al., 2011). According to Morel (1998) and field observations, is important to bear in mind the high bioturbation

and high mineral and chemical concentration of Fe (ferruginous level) and Mn, respectively, giving indications of a condensed level. This succession assembles the so-called "Niveau Thomel" that has been considered the local equivalent of the Italian "Bonarelli level" (Crumière, 1989; Fig. 2). Age control of the succession is based on combined foraminiferal, calcareous nannofossil and dinocyst biostratigraphic data (Crumière, 1991; Morel et al., 1998; Grosheny et al., 2006; Lignum, 2009) and correlation of the stable carbon isotope record with the Eastbourne reference section (Jarvis et al., 2011). The link to OAE2 is established by the $\delta^{13}C$ signature of the OM and inorganic material (Morel, 1998; Jarvis et al., 2011), displaying the worldwide recognized trend (~2.5‰ positive excursion; e.g. Arthur et al., 1988; Jenkyns et al., 1994; Tsikos et al., 2004; Erbacher et al., 2005; Sageman et al., 2006; Forster et al., 2008; Jenkyns, 2010; Jarvis et al., 2011; Dickson et al., 2017).

3. Materials and Methodologies

For this research 24 samples were collected belonging to the CTB succession of the Pont d'Issole section: eight from the *R. cushmani* biozone (four from Unit Th1 and three from Unit Th2; Jarvis et al., 2011), six from the *W. archaeocretacea* biozone (Unit Th2; Jarvis et al., 2011); and, ten from the *H. helvetica* biozone (Unit Th4; Jarvis et al., 2011).

3.1. Sample preparation

The isolation of the kerogen from the rock followed standard non-oxidative procedures (Tyson, 1995; Mendonça Filho et al. 2010, 2012). Samples were crushed (about 2 mm size) and underwent an acid treatment for the removal of carbonates, silicates and neoformed fluorides (HCl 37% for 18 h; HF 40% for 24 h; and, HCl 37% for 3 h, respectively), the solution was neutralized with distilled water between each step. Heavy liquid ($ZnCl_2$, density = 1.9 to 2 g/cm^3) was applied in order to concentrate the kerogen, eliminated with HCl (10%) drops, and then washed with distilled water. Strew slides and kerogen concentrate mounts were prepared using the isolated kerogen (sieved at 20 μm).

3.2. Geochemical analysis

3.2.1. Total organic carbon and total sulfur

Following acidification for removal of carbonates, total organic carbon (TOC) and total sulfur (TS) contents were determined with a LECO SC 144 analyzer (NCEA-C-1282,

2002; ASTM Standard D4239-08, 2008). Insoluble residue (IR) represents the fraction of the sample not eliminated by acidification.

3.2.2. Biomarkers

The bitumen was obtained by extraction in a Dionex® ASE 350 using dichloromethane as solvent. The extracts were fractioned into saturated, aromatic and NSO compounds by open-column chromatography with activated silica gel, using *n*-hexane, *n*-hexane/dichloromethane (8:2, v/v) and dichloromethane/methanol (1:1, v/v) as solvents, respectively. The saturated fraction was analyzed in an Agilent® 7890 gas chromatographer (GC) equipped with an Agilent® 7683 autosampler coupled to a triple quadrupole mass spectrometer (MS). The GC operated with a capillary column DB-5 Agilent (5% phenyl, 95% methylsiloxane, 30 m x 0.25 mm i.d., thickness 0.25 μm), at an initial temperature of 70ºC (1 min) raising up to 170ºC at 20ºC/min and 310ºC at 2ºC/min (10 min). Helium at a constant flow mode of 1.2 ml/min was used as the inert carrier gas. The injector ran at a constant temperature (280ºC) and the transfer line at 300ºC. MS ran with an ion source at 280ºC, interface temperature of 300ºC, quadrupole temperature of 150ºC and ionization voltage of 70 eV. The analyses were performed using selected ion monitoring for the analysis of the *n*-alkanes and terpanes (ions *m/z* 85 and *m/z* 191, respectively), and for the steranes (ions *m/z* 217 and *m/z* 218).

3.3. Palynofacies analysis

Optical microscopy (transmitted white (TWL) and incident blue (fluorescence mode – FM) lights) was used for a qualitative and quantitative examination of the kerogen. Palynofacies analysis was performed according to the dispersed OM classification described by Mendonça Filho and Gonçalves (2017), Mendonça Filho et al. (2010, 2012, 2016) and Tyson (1995). The organic particulate component quantitative data was recalculated and normalized for percentages.

3.4. Organic petrographic analyses

Optical petrography was performed on kerogen concentrate mounts prepared following the protocol described in section 3.1 and whole rock polished blocks (ISO 7404-2, 2009).

224 3.4.1. Organic matter reflectance

225 The OM reflectance measurements were performed using a Leica DM4000 microscope
226 equipped with a Discus-Fossil system, according to ASTM Standard D7708 (2014).
227 The OM reflectance was measured in various organic particles: vitrinite, hydrozoans, and
228 including reworked chitinozoans and graptolites. The identification of the particles in the
229 different preparations was based on their morphology and optical properties as proposed
230 and described by ICCP System 1994 (1998), Hartkopf-Fröder et al. (2015) and Fonseca
231 et al. (2018), and the hydrozoan reflectance value was calculated to equivalent vitrinite
232 reflectance using equation (1), as established by Bertrand and Malo (2012) and Hartkopf-
233 Fröder et al. (2015):

234 $$VR_{eq} = 0.6493*HR_r + 0.2126 \quad (1)$$

235 where VR_{eq} is the equivalent vitrinite reflectance and HR_r is the measured hydroid
236 random reflectance.
237

238 **4. Results and Interpretation**

239 *4.1. TOC and TS contents*

240 Total organic content ranges from 0.15 wt.% to 3.32 wt.%. Inside the "*Niveau Thomel*",
241 the black shales of the Unit Th3 display the highest values (average of 1.88 wt.%), while
242 the Unit Th2 exhibited the lowest percentages (average of 0.26 wt.%). The units Th1 and
243 Th4 show the average values for the "*Niveau Thomel*" (0.71 wt.% and 0.67 wt.%,
244 respectively; Table 1). Total sulfur values vary from 0.01 wt.% to 0.45 wt.%, with the
245 Unit Th3 displaying the highest percentages. The units Th1, Th2 and Th4 display the
246 same average value of 0.13 wt.%. The lowest value is observed in sample PIS1.5 at the
247 base of the section (Table 1). Insoluble residue varies between 13 wt.% and 60 wt.%, with
248 the black shales of the Unit Th3 exhibiting the highest mean percentages (52 wt.%) and
249 the lowest being registered at the base of the section with sample PIS1.5 (Table 1).

250 Table 1. Palynofacies and geochemical data of the Pont d'Issole section samples.

Sample	Lithology	Geochemistry			Palynofacies				APP plot (Tyson, 1995)	Interval
		TOC (wt.%)	Sulfur (wt.%)	IR (wt.%)	PHY (%)	AMO (%)	PAL (%)	ZOO (%)		
Th4										
PIS20	Marly limestone	0.21	0.06	14	2.1	45.2	50.1	2.6	VII	6
PIS19.6	Black Shale	1.34	0.22	37	1.1	79.2	18.2	1.6	VIII	
PIS19.5	Marl	0.25	0.02	23	8.1	17.1	73.1	1.8	V	
PIS19	Calcareous Marl	0.21	0.01	29	2.9	24.4	72.3	0.3	V	
PIS18.5	Dolomitized limestone	0.15	0.01	19	3.7	21.6	73.0	1.7	V	
PIS18	Marl	0.40	0.15	33	2.5	52.5	40.5	4.5	VII	5
PIS17.5	Marly limestone	0.25	0.10	18	2.6	43.9	46.2	7.3	VII	
PIS17	Black Shale	1.53	0.31	39	0.6	84.1	12.9	2.4	VIII	4
PIS16	Calcareous Marl	1.65	0.30	40	0.9	69.4	27.6	2.1	VIII	
Th3										
PIS15	Marl	1.99	0.23	43	0.6	85.5	10.9	2.9	VIII	
PIS14.5	Black Shale	3.32	0.45	54	0.4	91.5	6.9	1.3	IX	
PIS14	Black Shale	2.13	0.13	56	0.3	86.2	12.5	1.0	VIII	
PIS13	Black Shale	1.35	0.08	55	1.9	81.8	14.5	1.9	VIII	
PIS12	Calcareous Marl	0.60	0.22	50	3.3	76.5	18.2	2.1	VIII	
PIS11	Black Shale	1.89	0.31	52	0.5	88.9	10.3	0.3	VIII	
Th2										
PIS10	Marl	0.25	0.01	38	4.7	25.5	66.4	3.5	V	3
PIS9	Marly limestone	0.18	0.09	23	5.1	29.8	63.0	2.1	V	
PIS8	Calcareous marl	0.32	0.23	26	4.8	40.0	50.6	4.5	VII	2
PIS7.5	Calcareous marl	0.28	0.19	26	5.6	40.2	47.4	6.8	VII	
Th1										
PIS6.5	Calcareous marl	0.49	0.04	33	2.5	54.1	40.3	3.0	VII	
PIS5	Black Shale	1.30	0.38	50	1.8	57.1	34.1	6.9	VIII	
PIS3	Marl	0.53	0.09	60	3.0	42.3	49.8	5.0	VII	
PIS2.5	Marly limestone	0.53	0.02	40	7.3	28.7	62.5	1.5	V	1
PIS1.5	Limestone	0.16	0.01	13	7.2	7.2	83.8	1.9	V	

251 TOC: Total organic carbon (wt.%); IR: Insoluble residue (wt.%); PHY: Phytoclast Group; AMO:
252 Amorphous Group; PAL: Palynomorph Group; ZOO: Zooclast Group; APP plot: Tyson (1995)
253 kerogen groups ternary diagram.

254

255 *4.2. Kerogen characterization*

256 The petrographic analysis of the kerogen revealed the presence of two different fractions
257 of particulate OM. In section 4.2.1 the results of the palynofacies analyses of the
258 Cretaceous fraction are presented and in section 4.2.2 the reworked Paleozoic organic
259 components are described. It is important to emphasize that only the palynofacies results
260 (expressed on a reworked-components-free-basis), in conjunction with the geochemical
261 data, were used for paleoenvironmental interpretation purposes.

262

263 4.2.1. Palynofacies

264 Palynofacies analyses recorded the occurrence of OM components belonging to the four
265 kerogen groups throughout the section (Fig. 3, Table 1).

266 The Phytoclast Group shows low percentages throughout the sequence, reaching the
267 highest value in sample PIS1.5 at the base of the section (7.2%) and the lowest value in
268 the Unit Th3 (average 1.2%). In terms of non-opaque phytoclasts, the highest percentages
269 are of biostructured phytoclasts (NOB), with small percentages of non-biostructured
270 phytoclasts (NONB) being present. The NOB phytoclasts present no fluorescence, are
271 brown to dark brown under TWL, and can be classified as striped (Fig. 3, A), banded and
272 pitted (Fig. 3, B) NOB phytoclasts. The NONB phytoclasts display no fluorescence and
273 are dark brown under TWL. Opaque phytoclasts, cuticles and membranes are also present.
274 Opaque phytoclasts displaying devolatilization pores are present throughout the section,
275 with higher percentages at the top of the Unit Th4 (Fig. 3, C). Particles of sclerenchymatic
276 tissue (sclereids; Fig. 3, D) appear in sample PIS17.5 (Unit Th4). Cuticles, some
277 displaying distinguishable stomata, displayed light to dark brown color in TWL and an
278 orange color in FM (Fig. 3, E). Membranes, derived from branches of higher plants or
279 leaves, are very thin, displaying a dark brown to pale yellow in TWL and a yellow color
280 in FM (Fig. 3, F).

281 The Amorphous Group percentages fluctuate between 7.2% and 91.5%. The highest
282 values are recorded in the Unit Th3 (average 85.1%), whereas the lowest value is
283 observed at the base of the section (sample PIS1.5 - 7.2%). The AOM from this group is
284 derived from the microbiological reworking of marine microplankton (Fig. 3, G–H). The
285 AOM displays a heterogeneous feature, with the presence of palynomorph inclusions,
286 presenting diverse colors in FM (dark yellow to dark brown) and a light to dark brown
287 color in TWL. Unit Th3 samples, with the exception of sample PIS12, present AOM
288 particles of larger size (>320 μm), with a lighter matrix in TWL and higher fluorescence.

Some homogeneous gelified AOM components with hyaline aspect and sharp outlines are also observed in these samples (Fig. 3, I). Resin particles are also described.

The Palynomorph Group shows percentages varying between 6.9% and 83.8%, with higher percentages at the base of the section (sample PIS1.5) and lowest values in the Unit Th3 (average 12.2%). All palynomorph subgroups are present:

i) Sporomorphs are present throughout the section, with higher relative abundance in samples from the Unit Th3, being characterized by both pollen grains and spores. Pollen appear as single grains or in the form of agglomerates (dyads, tetrads and polyads) with diverse ornamentations, forms and dimensions. They present a light orange to orange color in TWL and are yellow to orange in FM. Bisaccate pollen grains are present, with higher relative abundances in samples from the Unit Th3 and base of Unit Th4 (Fig. 3, J). Specimens belonging to the genus *Classopollis* (grains, dyads and tetrads) were recognized throughout the section, with the exception of samples from the Unit Th2 where this genus disappears or exhibits only sporadic appearances (Fig. 3, K). Spores also exhibit diverse shapes, sizes and ornamentations (exhibiting most of the times the trilete mark). These components display a light orange to orange color in TWL and are orange to yellow in FM;

ii) Freshwater microplankton is characterized by *Botryococcus* sp. and Zygnemataceae specimens. *Botryococcus* sp. are brown in TWL and orange in FM (Fig. 3, L). Zygnemataceae specimens (especially of the genus *Spirogyra*) are yellow in FM and light brown in TWL (Fig. 3, M);

iii) The marine microplankton subgroup is characterized by dinoflagellate cysts, acritarchs and prasinophyte algae (*Pterospermaella* and *Tasmanites*). The dinoflagellate cyst assemblages are extremely diverse, especially in samples from the units Th1, Th2 and sample PIS 1.5, being dominated in these samples by the *Palaeohystrichophora infusorioides* (Fig. 3, N) with also a moderate frequency of *Oligosphaeridium* sp., *Spiniferites* sp. and *Odontochitina operculata*. In sample PIS 16, dinoflagellate cysts from the genus *Bosedinia* were observed (Fig. 3, O). They are transparent to very light orange in TWL and exhibit an intense green to yellow fluorescence. Acritarchs are mostly small sized (8.838.1 μm), light orange in TWL and yellow in FM. *Pterospermaella* specimens display the typical equatorial flange and exhibit a yellow fluorescence and a light brown color under TWL. Prasinophytes from the genus *Tasmanites* present a thick-walled, smooth and spherical shape, are brown in TWL and yellow in FM; and,

iv) The zoomorph subgroup components were identified as foraminiferal test-linings, scolecodonts and hydrozoan polypoid forms. Foraminiferal test-linings are brown to dark brown in TWL and present no fluorescence (Fig. 3, P). Hydrozoan polypoid forms are brown to dark brown in TWL and display no fluorescence. Scolecodonts exhibit no fluorescence and are light brown to brown in TWL (Fig. 3, Q).

The Zooclast Group is characterized by crustacean eggs (Fig. 3, R) and undifferentiated zooclasts. These particles present no fluorescence, are dark brown in TWL and display percentages varying from 0.3% to 7.3%, with the Unit Th2 showing the highest values (4.2%).

Fragmented particles of pyritized radiolarians are present in sample PIS17.5.

4.2.2. Reworked Organic Matter

The analysis of these samples revealed the occurrence of reworked OM, most significantly, graptolite fragments (middle Cambrian–Carboniferous; Clarkson, 2013; Fig. 4, A–B), chitinozoans (Early Ordovician–Late Devonian; Jansonius and Jenkins, 1978; Fig. 4, C–D) and Devonian naviform acritarchs (Combaz et al., 1967; Fig. 4, E). The graptolite debris exhibit no fluorescence and are dark brown in TWL. Their identification depends on the characteristic curving interthecal septa. Chitinozoa specimens display vesicle shape and aperture, sometimes with the presence of appendices, no fluorescence and a dark brown to black color in TWL. The Devonian naviform acritarchs are characterized by elongated naviform vesicles with rounded ends, no polar processes, and no surface ornamentation. These acritarchs present light brown color in TWL and yellow to brown color in FM. Other reworked particles include cuticles (Fig. 4, F–G), sporomorphs (Fig. 4, H–I), prasinophytes and Salviniaceae (massulae of freshwater spore fern) that display dark brown to black color under TWL and low intensity brown or no fluorescence. Round shaped particles (namely vitrinite) in plugs of kerogen, under reflected white light, were also identified.

4.3. Paleoenvironmental reconstruction

Based on the kerogen composition (including kerogen groups plot (APP) established by Tyson, 1995, modified by Mendonça Filho et al., 2010, 2012) and geochemical data, the Pont d'Issole sedimentary sequence was divided into six intervals for paleoenvironmental interpretation (Fig. 5, 6).

Interval 1 corresponds to the base of the sedimentary sequence, pre-OAE2 and base of Unit Th1 (samples PIS1.5 and PIS2.5; Fig. 7, A), is characterized by low TOC associated to a palynofacies association dominated by marine microplankton (mainly proto-peridinioid dinocysts) and with low AOM percentages. These, coupled to the high relative abundance of phytoclasts and zoomorphs, suggest an oxidizing environment (field V, APP plot), representing an aerobic system (oxic shelf) as regards to a microbial biofacies (*sensu*, Tyson, 1995), allowing for enhanced organic productivity (phytoplanktonic) that supported the primary and secondary consumers (zoomorphs) (Tyson, 1995; Mendonça Filho and Gonçalves, 2017). Evidence of an arid climate is supported by the presence of *Classopollis* sp. (Srivastava, 1976; Vakhrameyev, 1982; Tyson, 1995; Mendonça Filho et al., 2010).

The majority of Unit Th1 and base of Unit Th2, included in interval 2 (samples PIS3 to PIS8; Fig. 7, B), corresponds to a diminishing of oxygen availability, reaching mostly dysoxic conditions with episodes of anoxia (fields VII and VIII, APP plot), which represents a dysaerobic to anaerobic system (Tyson, 1995). This oxygen depleted zone is probably most of the time located at the sediment/water interface or inside the sediment (field VII, APP plot), reaching periodically the bottom water (field VIII, APP plot) (also proposed by Danzelle et al., 2018). This is suggested by a palynofacies co-dominated by AOM and palynomorphs (mainly proto-peridinioid dinocysts and zoomorphs) and a concomitant increase in TOC, especially at the base of the interval. The same trend observed in TOC content is followed by the IR values, indicating an increase in the non-carbonate (siliciclastic) sedimentation. This represents a system with oxygen availability, allowing the occurrence of benthic and pelagic organisms (foraminiferal test-linings and crustacean eggs), primary producers (phytoplankton) as the base of the food chain for the development of the primary and secondary consumers, the zoomorphs (Mendonça Filho et al., 2016; Mendonça Filho and Gonçalves, 2017). The oxygen limited zone allows the occurrence of anaerobic microbiological reworking (amorphization processes; Tyson, 1995; Mendonça Filho and Gonçalves, 2017). Paleoclimatic conditions are equivalent to the previous interval (arid climate) suggested by the presence of *Classopollis* sp. (Srivastava, 1976; Vakhrameyev, 1982; Tyson, 1995; Mendonça Filho et al., 2010).

Interval 3 consists of the majority of Unit Th2 (samples PIS9 and PIS10; Fig. 7, C), is characterized by a reoxygenation of the water column (field V, APP plot), representing a microbial biofacies of an aerobic system (Tyson, 1995). This interval represents a condensed level with high bioturbation and high concentration in mineral (iron oxide in

ferruginous level) and chemical proxies (Fe and Mn, respectively; Morel, 1998), that coupled to a decrease in AOM percentages, low TOC contents, low IR values and an increase in marine influence (highest percentage of dinocysts of the section) suggest an increase in water level (Tyson, 1995). The disappearance or only sporadic appearances of the genus *Classopollis* in these samples suggest a change in paleoclimate, with a possible decrease in temperature (Srivastava, 1976; Vakhrameyev, 1982; Tyson, 1995; Mendonça Filho et al., 2010).

Unit Th3 and the base of Unit Th4, corresponding to interval 4 (samples PIS11 to PIS17; Fig. 7, D), are represented by the establishment of an oxygen-stratified water column (field VIII, APP plot). This suggests the development of an oxic to dysoxic, sometimes anoxic, environment, representing a system that is aerobic to dysaerobic, at times anaerobic (Tyson, 1995). This is translated by TOC-rich sediments with a palynofacies assemblage largely dominated by marine-derived AOM, with low percentages of phytoclasts and palynomorphs. The system displays a water column with an upper level with normal oxygen concentrations, allowing for an increase in primary productivity, and a lower level restricted in oxygen availability that permits the anaerobic microbiological reworking (amorphization) of the marine components (Tyson, 1995; Mendonça Filho and Gonçalves, 2017). This oxygen stratification is possibly associated with a restriction (field IX, APP plot) connected to a shallowing-up trend well represented by the appearance of freshwater microplankton (*Botryococcus* sp. and Zygnemataceae) and of the dinoflagellate cyst *Bosedinia* sp., described by Prauss (2012) as having a freshwater affinity. An increase in detrital influx is suggested by high IR values and the amorphization of the marine microplankton, when compared to the well-preserved particles of freshwater microplankton that are transported into the system (Tyson, 1995). Arid climate is re-established until the end of the section with the presence of the genus *Classopollis* (Srivastava, 1976; Vakhrameyev, 1982; Tyson, 1995; Mendonça Filho et al., 2010).

Interval 5 is situated at the top of OAE2 (Unit Th4, samples PIS17.5 and PIS18; Fig. 7, E) and corresponds to a palynofacies co-dominated by AOM and palynomorphs (marine microplankton and zoomorphs). There is a decrease in TOC content and IR values coupled to a decrease in the amorphization of the marine components. This is possibly connected to a transfer of the redoxcline from the water column to the sediment-water interface (field VII, APP plot) (Tyson, 1995).

The post-OAE2 recovery , interval 6, (top Unit Th4, samples PIS18.5 to PIS20; Fig. 7, F) is characterized by a drop in AOM and a proliferation in palynomorph percentages (zoomorphs) coupled to a decrease in TOC content and IR values equivalent to the previous interval that represents the ultimate reoxygenation (field V, APP plot). This interval is marked also by episodic periods of reestablishment of dysoxic conditions (fields VII and VIII, APP plot) in the samples that present highest TOC content coupled to high AOM percentages (Tyson, 1995).

4.4. Organic matter reflectance

Reflectance measurements were performed in four different organic particles: chitinozoans, graptolites, hydrozoans and vitrinite. Chitinozoans display reflectance values ranging from 1.08% and 4.37% CR_r. Graptolites reflectance values vary from 0.89% to 5.89% GR_r. Hydrozoans display and average reflectance of 0.49% HR_r (0.53% VR_{eq}). Vitrinite presents an average reflectance of 0.29% R_r, whereas the reworked vitrinite population identified displays an average reflectance of 0.60% R_r.

4.5. Molecular composition

The molecular composition of the bitumen was characterized through the identification of the *n*-alkanes and of the molecular biomarkers (terpanes and steranes) in samples PIS1.5, PIS3, PIS6.5, PIS9, PIS10, PIS11, PIS14.5, PIS17 and PIS19.6 (Fig. 8). The biomarker signature of the analyzed samples is summarized in Table 2.

As suggested by the vitrinite random reflectance described previously, the OM of the samples presents very low maturity (R_r = 0.29%). This is corroborated by the presence of unsaturated compounds, biological ββ hopanes, monoaromatic steranes and monoaromatic anthrasteroids in the molecular fraction, and by the biomarkers ratios (Ts/(Ts+Tm), C29Ts/(H29+C29Ts), H31 S(R+S), M30/H30, C_{29} ααα S/(S+R), C_{29} ββ/(αα+ββ); Table 2). This low maturity affected the molecular parameters indicative of depositional environment conditions, namely Pr/Ph, Pr/*n*C17, Ph/*n*C18 and norhopane (C_{29})/hopane (C_{30}) ratios, with them not being in accordance with the organic petrographic data. A complete characterization of the *n*-alkanes and acyclic isoprenoids, terpanes and steranes is performed in the following sub-sections.

455 4.5.1. Normal alkanes and acyclic isoprenoids

456 The *n*-alkanes pattern displays a dominance of short chains (C_{15}–C_{19}) over the long chains
457 (C_{27}–C_{31}) in all samples. This can be associated to a predominance of algae and/plankton
458 or with high temperatures that resulted in the cracking of the long chain *n*-alkanes (e.g.
459 Tissot and Welte, 1984; Peters et al., 2005; Fig. 8).

460 Pristane (Pr) and phytane (Ph) were identified in all samples, with the acyclic isoprenoids
461 Pr/Ph ratio displaying values varying from 0.35 to 2.08 (Table 2). This ratio is usually
462 applied to the definition of the depositional environment redox conditions, but it is a
463 sensible parameter to other variables, namely the origin of the OM and, as in this case,
464 maturity (Volkman and Maxwell, 1986; ten Haven et al., 1987, 1988; Peters et al., 2005).
465 The majority of the samples displayed a dominance of Pr over C_{17} (except samples
466 PIS1.5, PIS9 and PIS10) and of C_{18} over phytane (except samples PIS11, PIS14.5 and
467 PIS17) (Fig. 8; Table 2).

468 The carbon preference index (CPI; Peters et al., 2005) presented values <1 in the majority
469 of the samples, with only sample PIS14.5 displaying a value ≈1 (Table 2). This suggests
470 that the OM is mainly of marine origin and that it is immature (Peters et al., 2005). Sample
471 PIS14.5 CPI value could indicate that the OM is mature; nevertheless, this parameter is
472 affected by the origin of the OM and needs to be corroborated by other parameters,
473 namely vitrinite reflectance (Peters et al., 2005).

474

475 4.5.2. Terpanes

476 The *m/z* 191 mass chromatogram displays the occurrence of tricyclic and tetracyclic
477 terpanes in the range C_{20}–C_{24} in low concentration in almost all samples, with the
478 exception of samples from interval 4 (PIS11, PIS14.5 and PIS17; Fig. 8). These
479 components are thought to characterize an input of higher plants and, therefore, the low
480 prevalence of these components suggests the dominance of marine OM (Peters et al.,
481 2005).

482 The pentacyclic terpanes of the hopane series showed a dominance of the C_{30} hopane.
483 The norhopane (C_{29})/hopane (C_{30}) ratio was <1 in all samples (Table 2). The presence of
484 sulfur can be related to the preferential preservation of C_{29} norhopane, being regularly
485 identified in sediments, such as carbonates, that display low iron availability (Blanc and
486 Connan, 1992). Danzelle et al. (2018) suggested such conditions for the deposition of
487 units Th1 and Th3 at Pont d'Issole but no increase in C_{29} norhopane is observed, maybe
488 due to the higher IR values observed in these units.

The ratio which determines the relative stability of the hopanes C_{27}, Ts/(Ts+Tm), presented values between 0.10 and 0.32, showing a dominance of the isomer Tm over Ts (Table 2). The C_{29}Ts/(C_{29} hopane+C_{29}Ts) ratio varied between 0.05 and 0.24, showing a higher predominance of the less stable H29 (Table 2). These two ratios were not determined for sample PIS14.5 as the components C_{27} 18α22,29,30-trisnorneohopane (Ts) and C_{29}Ts were not identified in this sample. The moretanes/hopanes ratio (M30/H30), highly specific for low maturity OM, displayed values between 0.25 and 0.53 (Table 2). The isomerization ratio of the homohopane C_{31}, 22S/(22S+22R), displayed values ranging from 0.17 to 0.34 (Table 2). All these ratios indicate that the OM is immature (Peters et al., 2005).

Neohop-13(18)-ene and 30-norneohop-13(18)-ene (except PIS1.5) together with ββ hopanes C_{30}–C_{32} and β-TNH were identified in all samples (Fig. 8). The presence of neohop-13(18)-ene can indicate a stratified water body, as it is a compound thought to derive from dwelling bacteria (at or below the chemocline). Nevertheless, gammacerane that is a compound characteristic of a stratified water column, usually associated with hypersalinity, was not identified (Peters et al., 2005; Sachse et al., 2011; Sinninghe Damsté et al., 2014). The identification of unsaturated compounds coupled to the biological ββ hopanes is a clear indication of the low thermal evolution of the OM (Peters et al., 2005; Sousa et al., 2019).

The m/z 191 fragmentogram of sample PIS14.5 displayed also the presence of monoaromatic steranes, monoaromatic anthrasteroids, 30-norhop-17(21)-ene, hop-17(21)-ene and hopenes in the range C_{33}–C_{34} (Fig. 8). The presence of these components, namely the monoaromatic steranes and monoaromatic antrasteroids, have already been described in immature Cretaceous black shales, together with the less stable ββ hopanes series and unsaturated hydrocarbons (hopenes and monosterenes), by Hussler et al. (1981) and Hussler and Albrecht (1983).

4.5.3. Steranes

The analysis of the m/z 217 fragmentogram showed the presence of cholestane (C_{27}), ergostane (C_{28}) and stigmastane (C_{29}) series. Regarding the C_{27}/C_{29} sterane ratio, only sample PIS1.5 shows value >1. A dominance of the C_{27} sterane can be linked to higher contributions of planktonic OM, while the C_{29} sterane suggests a higher continental contribution (Huang and Meinschein, 1979; Peters et al., 2005). However, as it is known

522 that marine algae produce both 27 and 29 sterols, the distribution of regular steranes as
523 source indicators must be used with caution (Moldowan et al., 1985; Peters et al., 2005).
524 The steranes isomerization ratio C_{29} ααα S/(S+R) values range from 0.05 to 0.24,
525 indicating that the 20R stereochemistry dominates over the 20S (Table 2). The C_{29}
526 ββ/(αα+ββ) ratio ranges between 0.36 e 0.42 (Table 2). Both isomerization ratios suggest
527 a low maturity for the OM (Peters et al., 2005). Diasteranes were identified in all samples
528 indicating the presence of clay in the rock (Peters et al., 2005).

Table 2. Molecular parameters of samples from the Pont d'Issole section.

Sample	*n*-alkanes				Terpanes						Steranes		
	Pr/Ph	Pr/*n*-C17	Ph/*n*-C18	CPI	Ts/Tm	C_{29}Ts/(Ts+Tm)	H31 S(S+R)	H29/H30	M30/H30	Ster/17α-Hop	C_{27}/C_{29} sterane	C_{29} S/(S+R)	C_{29} ββ/(αα+ββ)
Th4													
PIS19.6	1.66	2.49	0.94	0.94	0.10	0.05	0.19	0.38	0.47	2.28	0.90	0.14	0.36
PIS17	2.08	4.63	1.33	0.88	0.14	0.24	0.17	0.40	0.41	1.69	0.72	0.11	0.37
Th3													
PIS14.5	1.31	4.20	3.07	1.03	-	-	0.21	-	0.36	6.02	0.86	0.19	0.38
PIS11	1.12	3.30	1.98	0.80	0.32	0.22	0.20	0.28	0.53	2.42	0.67	0.11	0.38
Th2													
PIS10	0.63	0.72	0.50	0.51	0.17	0.20	0.28	0.56	0.40	1.53	0.79	0.24	0.39
PIS9	0.44	0.93	0.48	0.62	0.19	0.15	0.30	0.58	0.25	1.72	0.95	0.26	0.42
Th1													
PIS6.5	1.00	1.84	0.71	0.83	0.13	0.15	0.20	0.42	0.47	2.08	0.88	0.17	0.41
PIS3	1.03	1.34	0.59	0.80	0.13	0.15	0.22	0.44	0.44	2.16	0.83	0.13	0.37
PIS1.5	0.35	0.80	0.53	0.69	0.19	0.17	0.34	0.63	0.30	1.06	1.02	0.28	0.39

Pr: Pristane; Ph: Phytane; CPI: Carbon Preference Index [2*(nC_{23}+nC_{25}+nC_{27}+nC_{29})/ nC_{22}+2*(nC_{24}+nC_{26}+nC_{28})+ nC_{30}]; Ts: 22,29,30-Trisnorneohopane; Tm: 22,29,30-Trisnorhopane; C_{29}Ts: 18α(H)-Norneohopane; M30: C_{30} 17β,21α(H)-Hopane (Moretane); H29: C_{29} 17α(H),21α(H)-norhopane; H30: C_{30} 17α,21β(H)-Hopane; H31: C_{31} 17α(H),21β(H)-homohopane; (Ster/17α-hop): regular steranes consist of the C_{27}, C_{28}, C_{29} ααα(20S+20R) and αββ(20S+20R)/17α-hopanes consist of the C_{29} to C_{33} pseudo-homologue (including 22S and 22R epimers); C_{27}/C_{29} sterane: C_{27} ααα 20R/C_{29}ααα 20R; C_{29} S/(S+R): content of C_{29} ααα 20S/(20S +20R); C_{29} ββ/(αα+ββ): content of C_{29} ββ/(αα+ββ) (including 20S and 20R epimers).

5. Discussion

The organic record of the CTB at the Pont d'Issole section shows a shallowing-up marine system with an increase in restriction conditions at the deposition of organic-rich shales. Periods of stratified oxygen regimen in the water column (oxic to suboxic and dysoxic to anoxic) were identified, with organic richness in accordance with previous studies (Crumière, 1989; 1991; Morel, 1998; Jarvis et al., 2011; Danzelle et al., 2018; Raven et al., 2018).

5.1. Redox conditions and OM origin

Redox conditions throughout the section are broadly in accordance with already published data by Danzelle et al. (2018). The organic record shows that pre-OAE2 conditions are not favorable to high preservation of OM. This interval is characterized by an oxic water column with an assemblage dominated by the marine microplankton (Fig. 7, A). These conditions change throughout Unit Th1, with oxygen availability reaching dysoxic conditions, shown by the increase of AOM (Fig. 7, B). The dominance of proto-peridinioid cysts in the samples of Th1 and Th2 corroborate a pelagic context with limited nutrients influx from the shelf and not related to upwelling. Pearce et al. (2003) suggest that an increase of these peridinioid taxa could be related to an increased terrestrial nutrient flux, which could be connected to the increase in detrital influx observed especially at the base of Unit Th1. At the time of deposition of Unit Th2, a reoxygenation of the water column occurs, with dysoxic conditions disappearing and the water column becoming oxic to the top, culminating in the highest marine influence (Fig. 7, C). Unit Th3 and the base of Unit Th4 represent the most depleted oxygen conditions of the section, with the establishment of dysoxic to anoxic conditions, possibly due to restriction connected to a shallowing-up trend well represented by the appearance of freshwater microplankton (*Botryococcus* sp. and Zygnemataceae) and *Bosedinia* sp. (freshwater dinoflagellate cyst; Fig. 7, DE). This overall shallowing-up trend previously described is corroborated by interpretations already published by Grosheny et al. (2017), who suggest that the increase of accumulation rate in slope setting with the emplacement of turbidites is associated to an acceleration of the progradation of the Provence platform to the north. This would be associated with a S-N compressive tectonic pulse that began around the deposition of the Unit Th2 (Plenus Event) and was responsible for the reactivation of strike-slip faults. This tectonic pulse represents the beginning of the closure of the basin,

being possibly related to S-N compressional movement between Europe and Africa (Porthault, 1974; Bosworth et al., 1999; Grosheny et al., 2017).

At the top of Unit Th4, another reoxygenation of the water column occurs with the transition to more oxic conditions that are completely established post-OAE2 (Fig. 7, F). Some levels with high TOC and AOM percentages show some episodes of reestablishment of suboxic conditions at the top of the succession. At the top of this unit opaque phytoclasts displaying devolatilization pores were identified, which suggests that these particles originated by charcoalification (Tyson, 1995; Mendonça Filho and Gonçalves, 2017). Sclereids (sclerenchymatic tissue), formed by natural pyrolysis by the effect of high temperatures in the absence of oxygen that can occur in the middle of large natural wildfires, were also observed (Tyson, 1995; Mendonça Filho and Gonçalves, 2017). Therefore, at the time of deposition of Unit Th4, natural wildfires were occurring at/or near the terrestrial source area.

5.2. OM sulfurization

Samples from Unit Th3 are characterized by AOM with higher degree of preservation and by the presence of homogeneous gelified particles. This better preserved AOM evidently potentiates the TOC values observed in this unit (with the exception of sample PIS12). As previously suggested for the AOM in the Kimmeridge Clay by Boussafir et al. (1995), Tribovillard et al. (2001) and references therein, this difference in the AOM optical properties could be related to an early diagenetic process of sulfurization of the OM ("natural vulcanization"). This process is related to the incorporation of reduced sulfur into low-molecular-weight functionalized lipids, resulting in the production of resistant abiogenic "geopolymers" of high molecular weight, and ultimately leading to a sulfur-rich kerogen (e.g. Taylor et al., 1998; Tribovillard et al., 2001). This process has already been suggested as being at the origin of the organic-rich shales from units Th1 and Th3 at Pont d'Issole by Danzelle et al. (2018) and Raven et al. (2018, 2019), based on geochemical and isotopic studies. Although the petrographic features of the kerogen could suggest the occurrence of this process in sediments of Unit Th3, the AOM present in samples from Unit Th1 does not display the same optical characteristics. This suggests that, at Pont d'Issole, the OM sulfurization process only played a role in the maximization of the OM preservation in the organic-rich shales of Unit Th3.

In terms of the molecular composition, the low maturity of the samples, characterized by the biomarkers ratios and the presence of unsaturated compounds coupled to the

biological ββ hopanes, monoaromatic steranes, monoaromatic anthrasteroids, and hopenes, compromised the molecular parameters that give indications on the depositional environment. Nevertheless, the majority of the biomarkers related to OM source suggest a dominance of marine OM; which is in accordance with the petrographic observations that indicate a dominance of marine-derived AOM.

5.3. Plenus Cold Event

The paleoclimatic framework shows an arid climate (hot and dry) for the majority of the section, with a probable decrease in temperature in the Unit Th2 represented by the disappearance of the genus *Classopollis* or with only sporadic appearances. This cooling trend is coincidental with the described Plenus Cold Event, firstly suggested in this section by Jarvis et al. (2011) based on $\delta^{13}C$ data and later confirmed by Grosheny et al. (2017) through the *M. deltioensis* cooling ratio.

5.4. Reworked OM and thermal maturity

The reworked OM association identified at Pont d'Issole indicates that the majority of the reworked material dates from the Paleozoic (Ordovician–Carboniferous) and reveals detrital input, possibly in the distal part of turbiditic systems, in this context of deep basin (Grosheny et al., 2017). In accordance with geodynamic reconstructions (e.g. Schreiber et al., 2011), the deposition of clastic/reworked sediments, including OM, in the Late Cretaceous of the Subalpine Basin reflects the subaerial erosion of uplifted Hercynian massifs (Maures Massif for example; e.g. Gueirard et al., 1970; Boivin et al., 2012) and its Mesozoic cover as a response to the crustal compression associated with the Pyrenean-Provençal deformation phase. As previously mentioned, the tectonic disturbances around the CTB represent a pulse in the compressive trend between Africa and Europe (Grosheny et al., 2017). Thus, these results show the importance of the local paleogeographic context on the sedimentation and require a thoughtful choice of proxies used to propose paleoenvironmental reconstructions in relation with OAE2.

The differences between the reflectance values of the reworked (chitinozoans, graptolites, re-cycled vitrinite) and the autochtonous organic material (vitrinite and hydrozoans) show that the reworked components display higher reflectance values. This suggests a previous thermal history for the reworked OM comparing to the Pont d'Issole immature Cretaceous organic material. These results are in agreement with geochemical data, namely the molecular parameters described in section 4.5., and Rock-Eval pyrolysis published data

636 that displays an average T_{max} value of 420ºC for the organic-rich shales of this section
637 (Crumière, 1991; Javis et al., 2011). Nevertheless, it is important to emphasize the
638 difference between the vitrinite reflectance and the hydrozoan equivalent vitrinite values.
639 The equation used for the determination of the equivalent vitrinite reflectance of these
640 zoomorphs is most probably the cause for this discrepancy, as it was established for
641 Paleozoic hydroids. At the moment, no relationship for Cretaceous hydroids is available
642 on the literature with the most recent study being published by Fonseca al. (2018) for
643 Lower Jurassic hydroids.
644
645 *5.5. Organic-rich sedimentation control mechanisms*
646 Taking into account all information discussed previously, one can propose different
647 control mechanisms for the deposition of the two organic enrichment episodes at Pont
648 d'Issole (Unit Th1, and units Th3 and base of Th4). During the deposition of the Unit Th1
649 (first OM enrichment episode), OM deposition is controlled by global mechanisms
650 possibly connected to the triggering factors of OAE2, namely the high atmospheric CO_2
651 concentrations connected to the emplacement of Large Igneous Provinces that enhanced
652 a warm climate and the oxygen restriction in the oceans and atmosphere (e.g. Jones and
653 Jenkyns, 2001; Pucéat et al., 2003; Takashima et al., 2006; Forster et al., 2007; Friedrich
654 et al., 2012; Sinninghe Damsté et al., 2010; O'Brien et al., 2017; Danzelle et al., 2018).
655 On the other hand, the deposition of unit Th3 and the base of Unit Th4 (second OM
656 enrichment episode) is controlled mainly by local factors, namely by restriction
657 conditions developed in connection with the local tectonic framework and the beginning
658 stages of basin closure (Grosheny et al., 2017).
659
660 **6. Conclusions**
661 This study offers new evidence for the paleoenvironmental conditions during the CTB at
662 the Pont d'Issole section and a discussion about the mechanisms that control OAE2 in the
663 Subalpine Basin, based on a complete characterization of the organic fraction supported
664 by molecular composition and organic facies variability.
665 Two fractions of the organic association were identified: (i) Paleozoic reworked OM
666 originating from the erosion of uplifted Hercynian massifs having a much more complex
667 thermal history than the; (ii) autochthonous Cretaceous OM.
668 The Pont d'Issole section organic facies variability revealed a shallowing-up marine
669 system with oscillations in the redox conditions associated with periods of stratified

oxygen regimen and variability in the restriction conditions. OAE2 record exhibits the presence of two OM enrichment episodes that vary in depositional paleoenvironmental and geodynamic contexts. Unit Th1 (first OM enrichment episode) deposition reflects the global mechanisms associated to OAE2 and takes place in a high sea-level context, with a palynofacies association co-dominated by AOM and marine microplankton. At the time of deposition of Unit Th3 and the base of Unit Th4 (second OM enrichment episode) conditions are different, with the association largely dominated by AOM and with the occurrence of freshwater microplankton in a more restricted environment with low sea level. These conditions are favored by the regional tectonic framework with the beginning phases of basin closure. These two episodes are intercalated by the record of the Plenus Cold Event, where a reoxygenation of the water column and a probable drop in temperature is recorded.

Acknowledgements

The authors thank the team from the Laboratory of Palynofacies and Organic Facies of the Federal University of Rio de Janeiro (LAFO-UFRJ) for their technical support in sample preparation and all geochemical analyses, and the Laboratory of Organic Petrography of the ICT – Instituto de Ciências da Terra and the Department of Geosciences, Environment and Spatial Planning of the University of Porto. The authors also acknowledge the valuable contributions and suggestions of the reviewers.

References

Arthur, M.A., Dean, W.E., Pratt, L.M., 1988. Geochemical and climatic effects of increased marine organic carbon burial at the Cenomanian/Turonian boundary. Nature 335, 714–717. http://dx.doi.org/10.1038/335714a0.

ASTM Standard D4239-08, 2008. Standard Test Methods for Sulfur in the Analysis Sample of Coal and Coke Using High-Temperature Tube Furnace Combustion Methods. ASTM International, West Conshohocken, PA. http://dx.doi.org/10.1520/D4239-12.

ASTM Standard D7708, 2014. Standard Test Method for Microscopical Determination of Reflectance of Vitrinite Dispersed in Sedimentary Rocks. ASTM International, West Conshohocken, PA. http://dx.doi.org/10.1520/D7708-14.

Bertrand, R., Malo, M., 2012. Dispersed organic matter reflectance and thermal maturation in four hydrocarbon exploration wells in the Hudson Bay Basin: regional implications. Geological Survey of Canada Open File 7066, 1–52.

Blanc, P.L., Connan, J., 1992. Origin and occurrence of 25-norhopanes: a statistical study. Organic Geochemistry 18, 813–828.

Boivin, S., Laville, P., Sougy, J., 2012. Confirmation et description d'une espèce de graptolite dans l'île de Porauerolles (Var, France). Scientific reports of the Port-Cros national Park 26, 239-241.

Bordenave, M.L., Espitalié, L., Leplat, P., Oudin, J.L., Vandenbroucke, M., 1993. Screening techniques for source rock evaluation. In: Bordenave, M.L. (Ed.), Applied Petroleum Geochemistry. Editions Technip, Paris, pp. 217-278.

Bosworth, W., Guiraud, R., Kessler II, L.G., 1999. Late Cretaceous (ca. 84 Ma) compressive deformation of the stable platform of northeast Africa (Egypt): Farfield stress effects of the 'Santonian event' and origin of the Syrian arc deformation belt. Geology 27, 633-636.

Boussafir, M., Gelin, F., Lallier-Vergès, E., Derenne, S., Bertrand, P., Largeau, C., 1995. Electron microscopy and pyrolysis of kerogens from the Kimmeridge Clay Formation, UK: Source organisms, preservation processes, and origin of microcycles. Geochimica et Cosmochimica Acta 59 (18), 3731-3747. https://doi.org/10.1016/0016-7037(95)00273-3

Clarkson, E.N.K., 2013. Invertebrate Paleontology and Evolution. Blackwell Publishing, Oxford, UK, 468 pp.

Combaz, A., Lange, F.W., Pansart, J., 1967. Les «Leiofusidae» Eisenack, 1938. Review of Paleobotany and Palynology 1, 291-307.

Crumière, J.P., 1989. Crise anoxique à la limite Cénomanien-Turonien dans le bassin subalpin oriental (Sud-Est de la France). Relation avec l'eustatisme. Geobios 22 (1), 189-203. https://doi.org/10.1016/S0016-6995(89)80056-7.

Crumière, J.P., 1991. Les potentialités petroligènes des dépôts du Bassin Vocontien oriental (sud-est France) au Cenomanien-Turonien inférieur. Dynamiques de la sédimentation, de la préservation et de l'évolution de la matière organique, PhD. thesis, Université Claude-Bernard Lyon I, Lyon, France, 78 pp.

Crumière, J.P., Crumière-Airaud, C., Espitalié, J., 1990. Préservation cyclique de la matière organique amorphe des sédiments au passage Cénomanien-Turonien dans le Bassin vocontien (Sud-Est France). Contrôles paleo-océanographiques. Bulletin de la Société Géologique de France VI (3), 469–478. https://doi.org/10.2113/gssgfbull.VI.3.469.

Danzelle, J., Riquier, L., Baudin, F., Thomazo, C., Pucéat, E., 2018. Oscillating redox conditions in the Vocontian Basin (SE France) during Oceanic Anoxic Event 2 (OAE2). Chemical Geology 493, 136-152. https://doi.org/10.1016/j.chemgeo.2018.05.039.

Dickson, A.J., Saker-Clark, M., Jenkyns, H.C., Bottini, C., Erba, E., Russo, F., Gorbanenko, O., Naafs, B.A., Pancost, R.D., Robinson, S.A., van den Boorn, S., Idiz, E., 2017. A Southern Hemisphere record of global trace-metal drawdown and orbital modulation of organic-matter burial across the Cenomanian–Turonian boundary (Ocean

743 Drilling Program Site 1138, Kerguelen Plateau). Sedimentology 64, 186–203.
744 http://dx.doi.org/10.1111/sed.12303.

745 Du Vivier, A.D.C., Jacobson, A.D., Lehn, G.O., Selby, D., Hurtgen, M.T., Sageman,
746 B.B., 2015. Ca isotope stratigraphy across the Cenomanian-Turonian OAE 2: Links
747 between volcanism, seawater geochemistry, and the carbonate fractionation factor. Earth
748 and Planetary Science Letters 416, 121–131. https://doi.org/10.1016/j.epsl.2015.02.001.

749 Du Vivier, A.D.C., Selby, D., Sageman, B.B., Jarvis, I., Gröcke, D.R., Voigt, S., 2014.
750 Marine 187Os/188Os isotope stratigraphy reveals the interaction of volcanism and ocean
751 circulation during Oceanic Anoxic Event 2. Earth and Planetary Science Letters 389, 23–
752 33. http://dx.doi.org/10.1016/j.epsl.2013.12.024.

753 Erbacher, J., Friedrich, O., Wilson, P.A., Birch, H., Mutterlose, J., 2005. Stable organic
754 carbon isotope stratigraphy across Oceanic Anoxic Event 2 of Demerara Rise, Western
755 Tropical Atlantic. Geochemistry Geophysics Geosystems 6, Q06010.
756 http://dx.doi.org/10.1029/2004GC000850

757 Fonseca, C., Mendonça, J.O., Mendonça Filho, J.G., Lézin, C., Duarte, L.V., 2018.
758 Thermal maturity assessment study of the late Pliensbachian-early Toarcian organic-rich
759 sediments in southern France: Grands Causses, Quercy and Pyrenean basins. Marine and
760 Petroleum Geology 91, 338-349. https://doi.org/10.1016/j.marpetgeo.2018.01.017

761 Forster, A., Kuypers, M.M.M., Turgeon, S.C., Brumsack, H.-J., Petrizzo, M.R.,
762 Sinninghe Damste, J.S., 2008. The Cenomanian/Turonian oceanic anoxic event in the
763 South Atlantic: new insights from a geochemical study of DSDP Site 530A.
764 Palaeogeography, Palaeoclimatology, Palaeoecology 267, 256–283.
765 http://dx.doi.org/10.1016/j.palaeo.2008.07.006.

766 Forster, A., Schouten, S., Moriya, K., Wilson, P.A., Sinninghe Damsté, J.S., 2007.
767 Tropical warming and intermittent cooling during the Cenomanian/Turonian oceanic
768 anoxic event 2: sea surface temperature records from the equatorial Atlantic.
769 Paleoceanography 22, PA1219. http://dx.doi.org/10.1029/2006PA001349.

770 French, K.L., Hallmann, C., Hope, J.M., Schoon, P.L., Zumberge, J.A., Hoshino, Y.,
771 Peters, C.A., George, S.C., Love, G., Brocks, J.J., Buick, R., Summons, R.E., Reappraisal
772 of hydrocarbon biomarkers in Archean rocks. Proceedings of the National Academy of
773 Sciences of the United States of America 112 (19), 5915-5920.
774 www.pnas.org/cgi/doi/10.1073/pnas.1419563112.

775 Friedrich, O., Norris, R.D., Erbacher, J., 2012. Evolution of middle to Late Cretaceous
776 oceans – a 55 my record of Earth's temperature and carbon cycle. Geology 40, 107-110.
777 http://dx.doi.org/10.1130/G32701.1.

778 Frijia, G., Parente, M., 2008. Strontium isotope stratigraphy in the upper Cenomanian
779 shallow-water carbonates of the southern Apennines: short-term perturbations of marine
780 $^{87}Sr/^{86}Sr$ during the oceanic anoxic event 2. Palaeogeography, Palaeoclimatology,
781 Palaeoecology 261, 15-29. http://dx.doi.org/10.1016/j.palaeo.2008.01.003.

Ghassal, B.I., Littke, R., Sachse, V., Sindern, S., Schwarzbauer, J., 2016. Depositional environment and source rock potential of Cenomanian and Turonian sedimentary rocks of the Tarfaya Basin, Southwest Morocco. Geologica Acta 14 (4), 419-441. http://dx.doi.org/10.1344/GeologicaActa2016.14.4.6.

Gonçalves, P.A., Mendonça Filho, J.G., Silva, T.F., Flores, D., 2015. Palynofacies and source rock potential of Jurassic sequences on the Arruda sub-basin (Lusitanian Basin, Portugal). Marine and Petroleum Geology 59, 575-592.

Gonçalves, P.A., Mendonça Filho, J.G., Silva, T.F., Mendonça, J.O., Flores, D., 2014. The Mesozoic–Cenozoic organic facies in the Lower Tagus sub-basin (Lusitanian Basin, Portugal): Palynofacies and organic geochemistry approaches. Marine and Petroleum Geology 52, 42-56.

Gonçalves, P.A., Mendonça Filho, J.G., Mendonça, J.O., Silva, T.F., Flores, D., 2013. Paleoenvironmental characterization of a Jurassic sequence on the Bombarral sub-basin (Lusitanian basin, Portugal): Insights from palynofacies and organic geochemistry. International Journal of Coal Geology 113, 27-40

Grosheny, D., Beaudoin, B., Morel, L., Desmares, D., 2006. High-resolution biostratigraphy and chemostratigraphy of the Cenomanian/Turonian boundary event in the Vocontian Basin, southeast France. Cretaceous Research 27, 629-640. https://doi.org/10.1016/j.cretres.2006.03.005.

Grosheny, D., Ferry, S., Lécuyer, C., Thomas, A., Desmares, D., 2017. The Cenomanian-Turonian Boundary Event (CTBE) on the southern slope of the Subalpine Basin (SE France) and its bearing on a probable tectonic pulse on a larger scale. Cretaceous Research 72, 39-65. http://dx.doi.org/10.1016/j.cretres.2016.11.009.

Gueirard, S., Waterlot, G., Gherzi, A., Samat, M., 1970. Sur l'âge Llandovérien supérieur à Tarannonien inférieur des schistes à Graptolites du Fenouillet, massif des Maures (Var). Bulletin de la Société Géologique de France (7), XII, 2, 195-199.

Hartkopf-Fröder, C., Königshof, P., Littke, R., Schwarzbauer, J., 2015. Optical thermal maturity parameters and organic geochemical alteration at low grade diagenesis to anchimetamorphism: A review. International Journal of Coal Geology 150-151, 74-119. http://dx.doi.org/10.1016/j.coal.2015.06.005.

Hasegawa, T., 1997. Cenomanian-Turonian carbon isotope events recorded in terrestrial organic matter from northern Japan. Palaeogeography, Palaeoclimatology, Palaeoecology 130, 251–273. http://dx.doi.org/10.1016/S0031-0182(96)00129-0.

van Helmond, N.A.G.M., Ruvalcaba Baroni, I., Sluijs, A., Sinnighe Damsté, J.S., Slomp, C.P., 2014. Spatial extent and degree of oxygen depletion in the deep proto-North Atlantic basin during Oceanic Anoxic Event 2. Geochemistry, Geophysics, Geosystems 15, 4254-4266. http://dx.doi.org/10.1002/2014GC005528.

Hussler, G., Albrecht, P., 1983. C_{27}-C_{29} Monoaromatic anthrasteroid hydrocarbons in Cretaceous black shales. Nature 304, 262-263.

Hussler, G., Chappe, B., Wehrung, P., Albrecht, P., 1981. C_{27}-C_{29} ring A monoaromatic steroids in Cretaceous black shales. Nature 294, 556-558.

International Committee for Coal and Organic Petrology (ICCP), 1998. The new vitrinite classification (ICCP System 1994). Fuel 77 (5), 349-358. https://doi.org/10.1016/S0016-2361(98)80024-0.

ISO 7404-2, 2009. Methods for the petrographic analysis of coals — Part 2: methods of preparing coal samples. International Organization for Standardization, 12 pp.

Jansonius, J., Jenkins, W.A.M., 1978. Chitinozoa, in: Haq, B.V., Boersma, A. (Eds.), Introduction to marine micropaleontology. Elsevier, New York, 341-357.

Jarvis, I., Lignum, J.S., Gröcke, D.R., Jenkyns, H.C., Pearce, M.A., 2011. Black shale deposition, atmospheric CO_2 drawdown, and cooling during the Cenomanian-Turonian Oceanic Anoxic Event. Paleoceanography 26, PA3201. http://dx.doi.org/10.1029/2010PA002081.

Jenkyns, H.C., Gale, A.S., Corfield, R.M., 1994. Carbon- and oxygen-isotope stratigraphy of the English Chalk and Italian Scaglia and its palaeoclimatic significance. Geological Magazine 131, 1. http://dx.doi.org/10.1017/S0016756800010451.

Jenkyns, H.C., 2010. Geochemistry of oceanic anoxic events. Geochemistry, Geophysics, Geosystems 11, Q03004. http://dx.doi.org/10.1029/2009GC002788

Jones, C.E., Jenkyns, H.C., 2001. Seawater strontium isotopes, oceanic anoxic events, and seafloor hydrothermal activity in the Jurassic and Cretaceous. American Journal of Science 301, 112–149. http://dx.doi.org/10.2475/ajs.301.2.112.

Kerr, A.C., 1998. Oceanic plateau formation: a cause of mass extinction and black shales deposition around the Cenomanian-Turonian boundary? Journal of the Geological Society, London 155, 619-626.

Kuroda, J., Ogawa, N.O., Tanimizu, M., Coffin, M.F., Tokuyama, H., Kitazato, H., Ohkouchi, N., 2007. Contemporaneous massive subaerial volcanism and late cretaceous Oceanic Anoxic Event 2. Earth Planetary Science Letters 256, 211–223. http://dx.doi.org/10.1016/j.epsl.2007.01.027.

Leckie, R.M., Bralower, T.J., Cashman, R., 2002. Oceanic anoxic events and plankton evolution: biotic response to tectonic forcing during the mid-Cretaceous. Paleoceanography 17, 13-1. http://dx.doi.org/10.1029/2001PA000623.

Lignum, J., 2009. Cenomanian (Upper Cretaceous) palynology and chemostratigraphy: Dinoflagellate cysts as indicators of palaeoenvironmental and sea-level change, PhD. thesis, Kingston University London, Kingston upon Thames, United Kingdom, 582 pp.

Lüning, S., Kolonic, S., Belhadj, Z., Cota, L., Baric, G., Wagner, T., 2004. Integrated depositional model for the Cenomanian–Turonian organic-rich strata in North Africa. Earth-Science 64, 51-117. http://dx.doi.org/10.1016/S0012-8252(03)00039-4.

Mendonça Filho, J.G., Gonçalves, P.A., 2017. Organic Matter: Concepts and Definitions, Chapter 1, in: Suárez-Ruiz, I., Mendonça Filho, J.G. (Eds.), Geology: Current and Future

Developments. The Role of Organic Petrology in the Exploration of Conventional and Unconventional Hydrocarbon Systems. Bentham Science Publishers, United Arab Emirates, vol. 1, pp. 1-33.

Mendonça Filho, J.G., Menezes, T.R., Mendonça, J.O., Oliveira, A.D., Carvalho, M.A., Sant'Anna, A.J.; Souza, J.T., 2010. Palinofácies, in: Carvalho, I.S. (Ed.), Paleontologia, Rio de Janeiro, Interciência 2, pp. 379-413.

Mendonça Filho, J.G., Menezes, T.R., Mendonça, J.O., Oliveira, A.D., Silva, T.F., Rondon, N.F., Silva, F.S., 2012. Organic facies: Palynofacies and organic geochemistry approaches, in: Panagiotaras, D. (Ed.), Geochemistry - Earth's system processes. InTech, Rijeka, pp 211–248. http://dx.doi.org/10.5772/47928.

Mendonça Filho, J.G., Oliveira, A.D., Souza, J.T., Mendonça, J.O., Flores, D., 2016. The fossil record of hydrozoans in dispersed organic matter: a palynofacies and organic petrographic approach to kerogen characterization, in: Demchuk, T., O'Keefe, J., Gentzis, T., Curiale, J. (Eds.), TSOP The Society for Organic Petrology – ICCP International Committee for Coal and Organic Petrology – AASP The Palynological Society 2016 Joint Meeting Abstract Book, Houston, Texas, USA, pp. 84-86. Published as a supplement to AASP-The Palynological Society Newsletter 49-3, ISSN 0732-6041.

Moldowan, J.M., Seifert, W.K., Gallegos, E.L., 1985. Relationship between petroleum composition and depositional environment of petroleum source rocks. The American Association of Petroleim Geologists Bulletin 69 (8), 1255-1268.

Monteiro, F.M., Pancost, R.D., Ridgwell, A., Donnadieu, Y., 2012. Nutrients as the dominant control on the spread of anoxia and euxinia across the Cenomanian–Turonian oceanic anoxic event (OAE2): model-data comparison. Paleoceanography 27, PA4209. http://dx.doi.org/10.1029/2012PA002351.

Morel, L., 1998. Stratigraphie à haute résolution du passage Cénomanien-Turonien. Thèse de l'Université Pierre et Marie Curie, Paris VI, 224pp.

Mort, H.P., Adatte, T., Föllmi, K.B., Keller, G., Steinmann, P., Matera, V., Berner, Z., Stüben, D., 2007. Phosphorus and the roles of productivity and nutrient recycling during oceanic anoxic event 2. Geology 35, 483–486. http://dx.doi.org/10.1130/G23475A.1.

O'Brien, C.L., Robinson, S.A., Pancost, R.D., Damsté, J.S.S., Schouten, S., Lunt, D.J., Alsenz, H., Bornemann, A., Bottini, C., Brassell, S.C., Farnsworth, A., Forster, A., Huber, B.T., Inglis, G.N., Jenkyns, H.C., Linnert, C., Littler, K., Markwick, P., McAnena, A., Mutterlose, J., Naafs, B.D.A., Püttmann, W., Sluijs, A., van Helmond, N.A.G.M., Vellekoop, J., Wagner, T., Wrobel, N.E., 2017. Cretaceous sea-surface temperature evolution: constraints from TEX86 and planktonic foraminiferal oxygen isotopes. Earth-Science Reviews 172, 224-247. http://dx.doi.org/10.1016/j.earscirev.2017.07.012.

Pearce, M.A., Jarvis, I., Swan, R.H., Murphy, A.M., Tocher, B.A., Edmunds, W.M., 2003. Integrating palynological and geochemical data in a new approach to palaeoecological studies: Upper Cretaceous of the Banterwick Barn Chalk borehole, Berkshire, UK. Marine Micropaleontology 47, 271-306.

900 Peters, K.E., Cassa, M.R., 1994. Applied source rock geochemistry. In: Magoon, L.B.,
901 Dow, W.G. (Eds.), The petroleum system – from source to trap. American Association of
902 Petroleum Geologists Memoir 60, Tulsa, pp. 93-120.

903 Peters, K.E., Walters, C.C., Moldowan, J.M., 2005. The Biomarker Guide. Volume 1:
904 Biomarkers and Isotopes in the Environment and Human History. Volume 2: Biomarkers
905 and Isotopes in Petroleum Exploration and Earth History. 2nd Edition, Cambridge
906 University Press, New York, 1132 p.

907 Pogge von Strandmann, P.A.E., Jenkyns, H.C., Woodfine, R.G., 2013. Lithium isotope
908 evidence for enhanced weathering during Oceanic Anoxic Event 2. Nat. Geosci. 6, 668–
909 672. http://dx.doi.org/10.1038/ngeo1875.

910 Porthault, B., 1974. Le Crétacé supérieur de la 'Fosse vocontienne' et des régions
911 limitrophes (France Sud-Est). Thèse Doct.. Etat Université de Lyon. Available from:
912 https://hal.archives-ouvertes.fr/.

913 Prauss, M.L., 2012. Potential freshwater dinocysts from marine upper Cenomanian to
914 upper Coniacian strata of Tarfaya, northwest Africa: Three new species of Bosedinia.
915 Cretaceous Research 37, 285-290.

916 Pucéat, E., Lécuyer, C., Sheppard, S.M.F., Dromart, G., Reboulet, S., Grandjean, P.,
917 2003. Thermal evolution of Cretaceous Tethyan marine waters inferred from oxygen
918 isotope composition of fish tooth enamels. Paleoceanography 18, 1029.
919 http://dx.doi.org/10.1029/2002PA000823.

920 Raven, M.R., Fike, D.A., Bradley, A.S., Gomes, M.L., Owens, J.D., Webb, S.A., 2019.
921 Paired organic matter amd pyrite $\delta^{34}S$ records reveal mechanisms of carbon, sulfur, and
922 iron cycle disruption during Ocean Anoxic Event 2. Earth and Planetary Science Letters
923 512, 27-38. https://doi.org/10.1016/j.epsl.2019.01.048.

924 Raven, M.R., Fike, D.A., Gomes, M.L., Webb, S.M., Bradley, A.S., McClelland, H.O.,
925 2018. Organic carbon burial during OAE2 driven by changes in the locus of organic
926 matter sulfurization. Nature Communications 9, 3409. http://dx.doi.org/10.1038/s41467-
927 018-05943-6.

928 Sachse, V.F., Littke, R., Heim, S., Kluth, O., Schober, J., Boutib, L., Jabour, H., Perssen,
929 F., Sindern, S., 2011. Petroleum source rocks of the Tarfaya Basin and adjacent areas,
930 Morocco. Organic Geochemistry 42, 209-227.
931 http://dx.doi.org/10.1016/j.orggeochem.2010.12.004.

932 Sageman, B.B., Meyers, S.R., Arthur, M.A., 2006. Orbital time scale and new C-isotope
933 record for Cenomanian–Turonian boundary stratotype. Geology 34, 125–128.

934 Schlanger, S.O., Arthur, M.A., Jenkyns, H.C., Scholle, P.A., 1987. The Cenomanian-
935 Turonian Oceanic Anoxic event, I. Stratigraphy and distribution of organic carbon-rich
936 beds and the marine $\delta^{13}C$ excursion, in: Brooks, J., Fleet, A.J. (Eds.), Marine Petroleum
937 Source Rocks. Geological Society London Special Publications 26, pp. 371–399.

Schlanger, S.O., Jenkyns, H.C., 1976. Cretaceous oceanic anoxic event: causes and consequences. Geol. Mijnbouw 55, 179–188.

Scholle, P.A., Arthur, M.A., 1980. Carbon isotope fluctuations in Cretaceous pelagic limestones: potential stratigraphic and petroleum exploration tool. AAPG Bull. 64, 67–87.

Schreiber, D., Giannerini, G., Lardeaux, J., 2011. The Southeast France basin during Late Cretaceous times: The spatiotemporal link between Pyrenean collision and Alpine subduction. Geodinamica Acta 24/1, 21-35. http://dx.doi.org/10.3166/ga.24.21-35.

Sinninghe Damsté, J.S., van Bentum, E.C., Reichart, G.J., Pross, J., Schouten, S., 2010. A CO_2 decrease-driven cooling and increased latitudinal temperature gradient during the mid-Cretaceous Oceanic Anoxic Event 2. Earth Planetary Science Letters 293, 97–103. http://dx.doi.org/10.1016/j.epsl.2010.02.027.

Sinninghe Damsté, J.S., Kuypers, M.M.M., Pancost, R.D., Schouten, S., 2008. The carbon isotopic response of algae, (cyano)bacteria, archaea and higher plants to the late Cenomanian perturbation of the global carbon cycle: Insights from biomarkers in black shales from the Cape Verde Basin (DSDP Site 367). Organic Geochemistry 39, 1703-1718. http://dx.doi.org/10.1016/j.orggeochem.2008.01.012.

Sinninghe Damsté, J.S., Schouten, S., Volkman, J.K., 2014. C_{27}–C_{30} neohop-13(18)-enes and their saturated and aromatic derivatives in sediments: Indicators for diagenesis and water column stratification. Geochimica et Cosmochimica Acta 133, 402-421. http://dx.doi.org/10.1016/j.gca.2014.03.008.

Sinton, C.W., Duncan, R.A., 1997. Potential links between ocean plateau volcanism and global ocean anoxia at the Cenomanian-Turonian boundary. Econ. Geol. 92, 836–842. http://dx.doi.org/10.2113/gsecongeo.92.7-8.836.

Snow, L.J., Duncan, R.A., Bralower, T.J., 2005. Trace-element abundances in the Rock Canyon Anticline, Pueblo, Colorado, marine sedimentary section and their relationship to Caribbean plateau construction and oxygen anoxic event 2. Paleoceanography 20, PA3005. http://dx.doi.org/10.1029/2004PA001093.

Sousa, E.S., Sousa Júnior, G.R., Silva, A.F., Reis, F.A.M., de Sousa, A.A.C., Cioccari, G.M., Capilla, R., Souza, I.V.A.F., Imamura, P.M., Rodrigues, R., Lopes, J.A.D., de Lima, S.D., 2019. Biomarkers in Cretaceous sedimentary rocks from the Codó Formation – Parnaíba Basin: Paleoenvironmental assessment. Journal of South American Earth Sciences 92, 265-281. https://doi.org/10.1016/j.jsames.2019.03.025.

Srivastava, S.K., 1976. The fossil pollen genus Classopollis. Lethaia 9, 437–457. http://dx.doi.org/10.1111/j.1502-3931.1976.tb00985.x.

Takashima, R., Nishi, H., Huber, B., Leckie, R.M., 2006. Greenhouse world and the Mesozoic Ocean. Oceanography 19, 82–92. http://dx.doi.org/10.5670/oceanog.2006.07.

Takashima, R., Nishi, H., Hayashi, K., Okada, H., Kawahata, H., Yamanaka, T., Fernando, A.G., Mampuku, M., 2009. Litho-, bio- and chemostratigraphy across the Cenomanian/Turonian boundary (OAE 2) in the Vocontian Basin of southeastern France.

978 Palaeogeography, Palaeoclimatology, Palaeoecology 273, 61-74.
979 http://dx.doi.org/10.1016/j.palaeo.2008.12.001.

980 Taylor, G.H., Teichmüller, M., Davis, A., Diessel, C.F.K., Littke, R., Robert, P., 1998.
981 Organic Petrology. Gebrüder Borntraeger, Berlin, 704 pp.

982 Ten Haven, H.L., Leeuw, J.W., Rullkötter, J., Sinninghe Damsté, J.S., 1987. Restricted
983 utility of the pristane/phytane ratio as a paleoenvironmental indicator. Nature 330, 641-
984 643.

985 Ten Haven, H.L., Leeuw, J.W., Rullkötter, J., Sinninghe Damsté, J.S., 1988.
986 Pristane/phytane ratio as an environmental indicator. Nature 333, 604.

987 Tissot, B., Welte, D.H., 1984. Petroleum Formation and Occurrence. Springer Verlag,
988 New York. 699 pp.

989 Trabucho Alexandre, J., Tuenter, E., Henstra, G.A., van der Zwan, K.J., van de Wal,
990 R.S.W., Dijkstra, H.A., de Boer, P.L., 2010. The mid-Cretaceous North Atlantic nutrient
991 trap: Black shales and OAEs. Paleoceanography 25, PA4201.
992 http://dx.doi.org/10.1029/2010PA001925.

993 Tribovillard, N., Bialkowski, A., Tyson, R.V., Lallier-Vergès, E., Deconinck, J.-F., 2001.
994 Organic facies variation in the late Kimmeridgian of the Boulonnais area (northernmost
995 France). Marine and Petroleum Geology 18, 371-389. https://doi.org/10.1016/S0264-
996 8172(01)00006-X.

997 Tsikos, H., Jenkyns, H.C., Walsworth-Bell, B., Petrizzo, M.R., Forster, A., Kolonic, S.,
998 Erba, E., Premoli Silva, I., Baas, M., Wagner, T., Sinninghe Dameste, J.S., 2004. Carbon-
999 isotope stratigraphy recorded by the Cenomanian–Turonian Oceanic anoxic event:
1000 correlation and implications based on three key localities. Journal of the Geological
1001 Society, London 161, 711–719.

1002 Turgeon, S.C., Creaser, R.A., 2008. Cretaceous oceanic anoxic event 2 triggered by a
1003 massive magmatic episode. Nature 454, 323–326. http://dx.doi.org/10.1038/nature07076.

1004 Tyson, R.V., 1995. Sedimentary Organic Matter. Organic facies and palynofacies.
1005 Chapman and Hall, London. http://dx.doi.org/10.1007/978-94-011-0739-6.

1006 United States Environmental Protection Agency (U.S.EPA), 2002. Methods for the
1007 Determination of Total Organic Carbon (TOC) in Soils and Sediments. Ecological Risk
1008 Assessment Support Center. NCEA-C-1282. Office of Research and Development, Las
1009 Vegas.

1010 Vakhrameyev, V.A., 1982. Classopollis pollen as an indicator of Jurassic and Cretaceous
1011 climates. International Geology Review 24-10, 1190–1196.

1012 Volkman, J.K., Maxwell, J.R., 1986. Acyclic isoprenoids as biological markers, in: Johns,
1013 R.B. (Ed.), Biological Markers in the Sedimentary Record. Elsevier, Amsterdam, pp. 1-
1014 42

1015 Zheng, X.-Y., Jenkyns, H.C., Gale, A.S., Ward, D.J., Henderson, G.M., 2016. A climatic
1016 control on reorganization of ocean circulation during the mid-Cenomanian event and

Cenomanian-Turonian oceanic anoxic event (OAE 2): Nd isotope evidence. Geology 44, 151–154. http://dx.doi.org/10.1130/G37354.1.

Figure 1

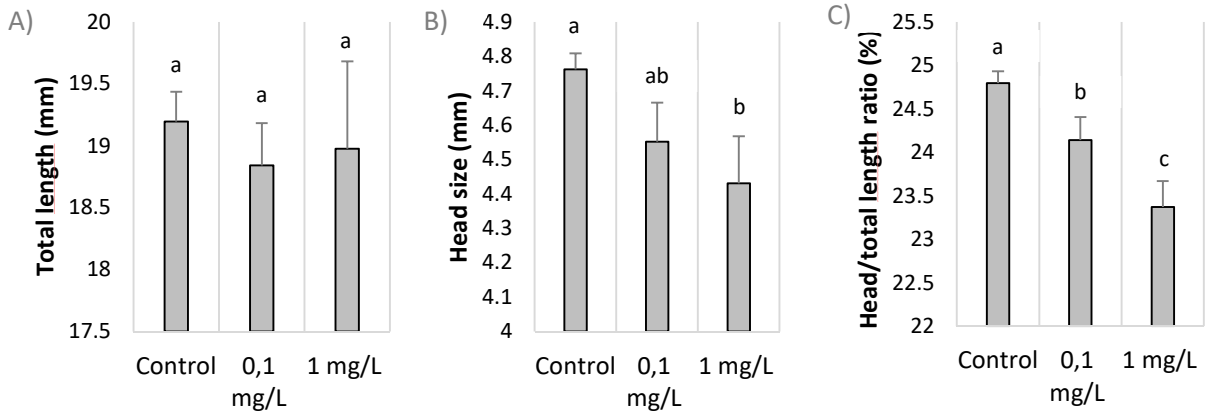
A)
Total length (mm)
20
19.5
19
18.5
18
17.5
a
a
a
Control
0,1 mg/L
1 mg/L
B)
Head size (mm)
4.9
4.8
4.7
4.6
4.5
4.4
4.3
4.2
4.1
4
a
ab
b
Control
0,1 mg/L
1 mg/L
C)
Head/total length ratio (%)
25.5
25
24.5
24
23.5
23
22.5
22
a
b
c
Control
0,1 mg/L
1 mg/L

Figure 2

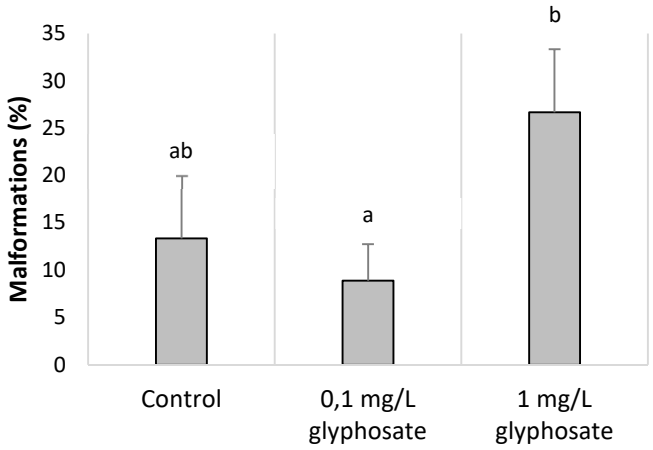
Malformations (%)
35
30
25
20
15
10
5
0
ab
a
b
Control
0,1 mg/L glyphosate
1 mg/L glyphosate

Figure 3

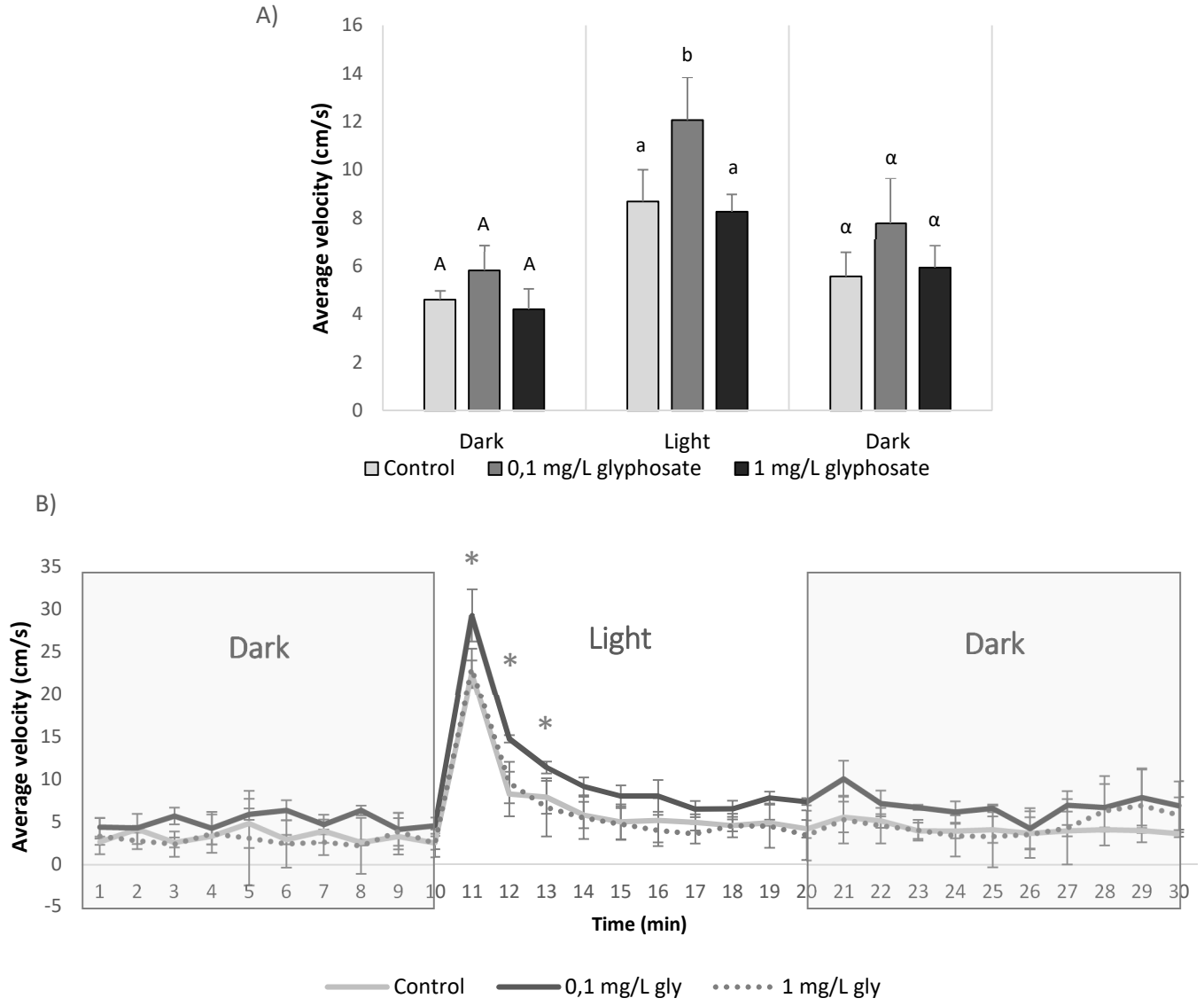
A)
Average velocity (cm/s)
16
14
12
10
8
6
4
2
0
A
A
A
a
b
a
α
α
α
Dark
Light
Dark
Control
0,1 mg/L glyphosate
1 mg/L glyphosate
B)
Average velocity (cm/s)
35
30
25
20
15
10
5
0
-5
Dark
Light
Dark
*
*
*
1 2 3 4 5 6 7 8 9 10 11 12 13 14 15 16 17 18 19 20 21 22 23 24 25 26 27 28 29 30
Time (min)
Control
0,1 mg/L gly
1 mg/L gly

Figure 4

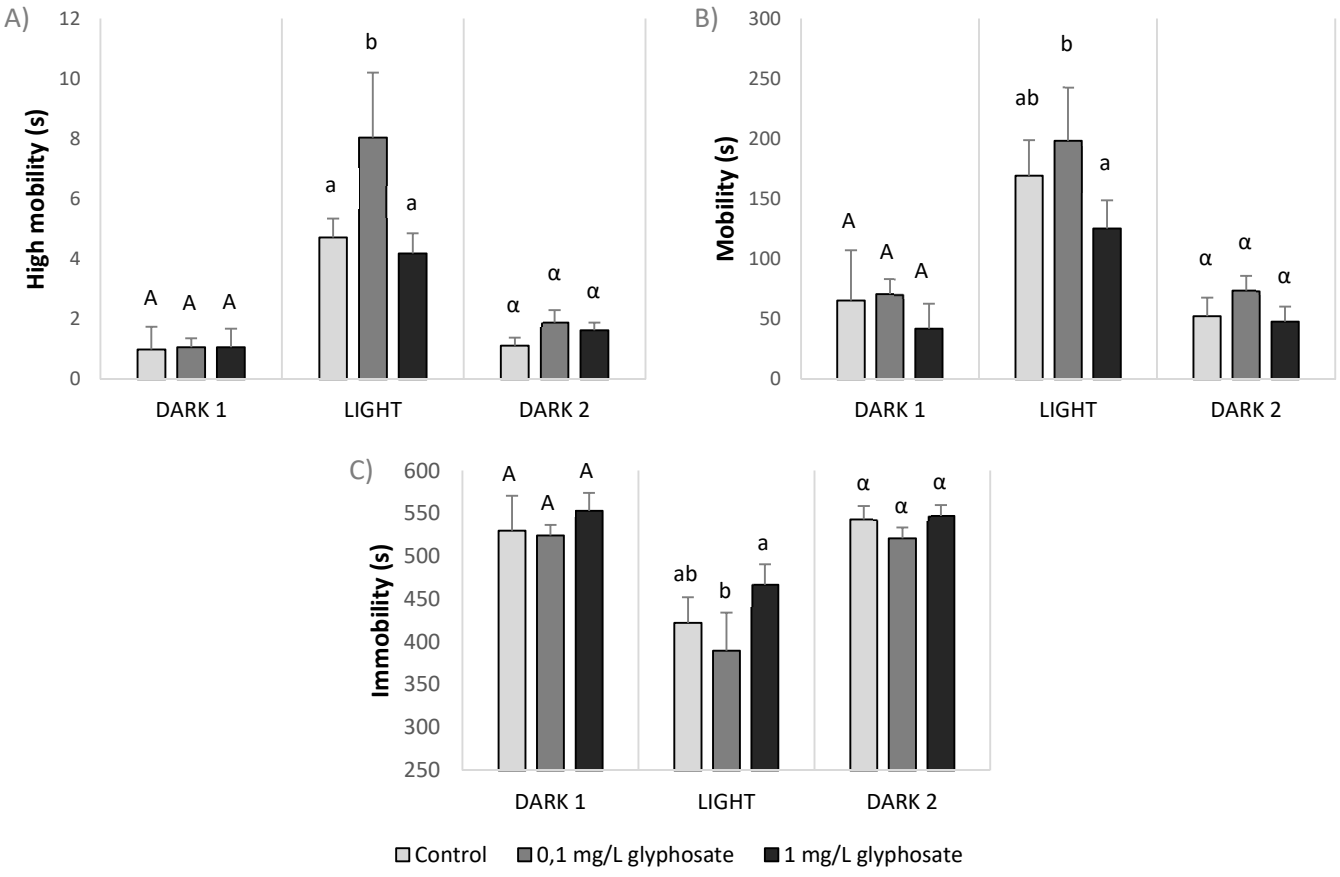
A)
High mobility (s)
12
10
8
6
4
2
0
A A A
a b a
α α α
DARK 1
LIGHT
DARK 2
B)
Mobility (s)
300
250
200
150
100
50
0
A A A
ab b a
α α α
DARK 1
LIGHT
DARK 2
C)
Immobility (s)
600
550
500
450
400
350
300
250
A A A
ab b a
α α α
DARK 1
LIGHT
DARK 2
Control
0,1 mg/L glyphosate
1 mg/L glyphosate

Figure 5

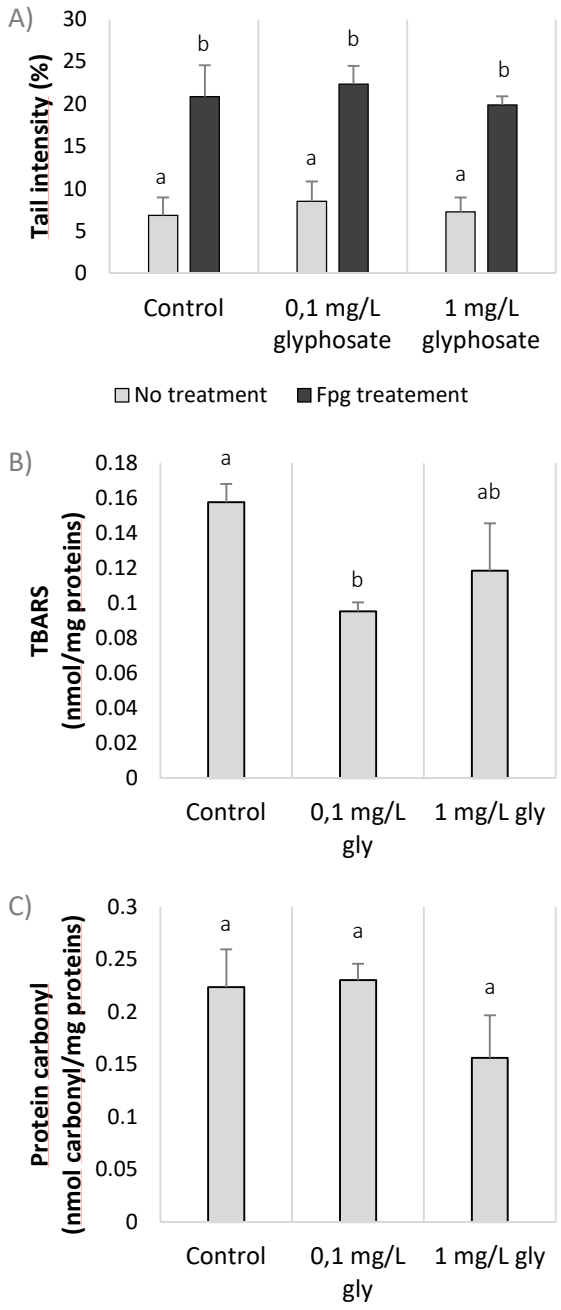
A)
Tail intensity (%)
30
25
20
15
10
5
0
a
b
a
b
a
b
Control
0,1 mg/L glyphosate
1 mg/L glyphosate
No treatment
Fpg treatement
B)
TBARS (nmol/mg proteins)
0.18
0.16
0.14
0.12
0.1
0.08
0.06
0.04
0.02
0
a
b
ab
Control
0,1 mg/L gly
1 mg/L gly
C)
Protein carbonyl (nmol carbonyl/mg proteins)
0.3
0.25
0.2
0.15
0.1
0.05
0
a
a
a
Control
0,1 mg/L gly
1 mg/L gly

Figure 6

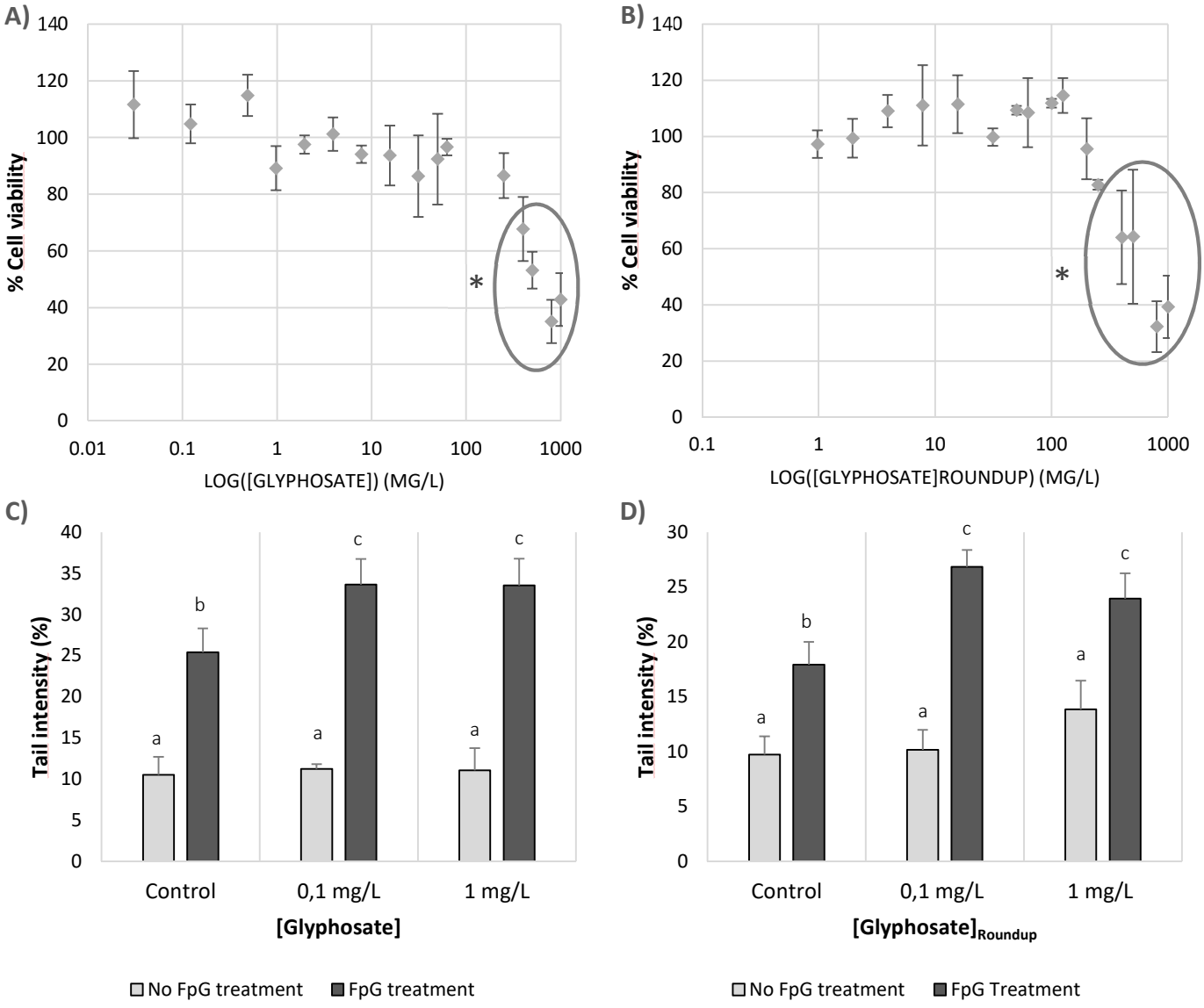
A)
% Cell viability
LOG([GLYPHOSATE]) (MG/L)
B)
% Cell viability
LOG([GLYPHOSATE]ROUNDUP) (MG/L)
C)
Tail intensity (%)
Control
0,1 mg/L
1 mg/L
[Glyphosate]
No FpG treatment
FpG treatment
D)
Tail intensity (%)
Control
0,1 mg/L
1 mg/L
[Glyphosate]Roundup
No FpG treatment
FpG Treatment